Parametric optimization of wear parameters of hybrid composites (LM6/B$_4$C/fly ash) using Taguchi technique

Jayavelu Udaya Prakash[1], Subramani Ananth[2],
Sunder Jebarose Juliyana[1], Robert Cep[3], Nitin Khedkar[4],
Sachin Salunkhe[1]*, Emad Abouel Nasr[5] and Ali Kamrani[6]

[1]Department of Mechanical Engineering, Vel Tech Rangarajan Dr. Sagunthala R&D Institute of Science and Technology, Chennai, India, [2]Department of Mechanical Engineering, Vardhaman College of Engineering, Hyderabad, India, [3]Department of Machining Assembly and Engineering Metrology, Faculty of Mechanical Engineering, VSB-Technical University of Ostrava, Ostrava-Poruba, Czechia, [4]Symbiosis International University, Pune, India, [5]Department of Industrial Engineering, College of Engineering, King Saud University, Riyadh, Saudi Arabia, [6]Industrial Engineering Department, College of Engineering, University of Houston, Houston, TX, United States

Wear is prominent in sliding components, so tribology property plays a major role in automotive as well as in the aerospace industries. In this work, Aluminium alloy LM6/B$_4$C/Fly Ash hybrid composites with three different weight percentages of reinforcement were fabricated using the low-cost stir casting technique, and the experiments were conducted based on the Design of Experiments (DoE) approach and optimized using Taguchi's Signal to noise ratio (S/N) analysis. The analysis was conducted with process parameters like Sliding Speed (S), Sliding distance (D), load (L) and reinforcement percentage (R %), the responses are Coefficient of Friction (COF) and Specific wear rate (SWR). Aluminum alloy reinforced with 9 wt% hybrid (LM6 + 4.5% B$_4$C + 4.5% Fly Ash) has a low density and high hardness compared with other composites and base alloys. The optimum parameters for obtaining minimum SWR are S - 1 m/s, D - 500 m, L - 45 N, and R% - 6 wt% Hybrid (3% Fly ash and 3% boron carbide). The optimum parameters for obtaining minimum COF are S - 1.5 m/s, D - 500 m, L - 30 N, and R% −9 wt% Hybrid (4.5% Fly ash and 4.5% boron carbide). Load (28.34%) is the most significant parameter for obtaining minimum SWR, and DL (31.62%) for obtaining minimum COF. SEM images of the worn pins show the various wear mechanisms of the AMCs. The hybrid composite produced is new and these may be used for piston liner and brake pad applications.

KEYWORDS

AMCs, wear, pin-on-disc, Taguchi technique, anova

1 Introduction

Composite materials are renowned for possession of high strength and lightweight. Composite material properties are influenced by different factors, which include matrix composition, reinforcement materials, volume fraction, form, and size of the particles (Idrisi and Mourad, 2019). Aluminium Matrix Composites (AMCs) are recently identified as the most promising material for high-tech functional and structural purposes widely used in defense, automobile industries, and Sports Equipment recreation (Bhaskar et al., 2018). The

stir casting process is recommended for bulk manufacturing among the numerous procedures used to synthesize metal matrix composites. To achieve the necessary qualities, researchers supplemented the Al matrix with various metallic, non-metallic, and ceramic components (Ananth et al., 2021). The employment of AMCs in the transportation industry is necessary and beneficial as environmental standards become more rigorous and a focus on greater fuel efficiency is placed (Suresh et al., 2018).

Today, scientists have developed several materials with several combinations and in different manufacturing methodologies. All the research focuses on a unique way of covering several properties with the help of adding a minimum quantity of superior material with lightweight parent material. One of the best examples is aluminum; its reinforcement provides less wear, high hardness, toughness, and improved strength equal to the superior material with cost-effectiveness. Analyzed different ratios of ceramic material 16% with AMC, gave high tensile strength of $223 \, N/mm^2$, and amplified the material's compressive strength. The tribological properties, such as hardness, wear, and COF, were enhanced by the occurrence of ceramic material, and the uniform distribution of reinforcement was confirmed by FESEM and XRD pattern (Aherwar et al., 2020).

The stir casting method is a prevalent and the most affordable way to produce AMCs with the required properties. AMCs provide increased tensile strength and reduced wear rate of the material. Three different samples were prepared by Venkatachalam and Kumaravel; the first two samples show improved tensile strength with more percentage of elongation and also a higher hardness of 75.43HV in the combination of 5% SiC+5% Fly ash. 10% SiC shows a stable coefficient of friction and three times less than the mild steel's strength-to-weight ratio; this type of AMC is used in automobile and aerospace industries (Venkatachalam and Kumaravel, 2017). Enhanced development of AMCs is the prime motto for researchers in several methodologies. Adding the B4C with AMCs increases the fatigue strength from 116.4 MPa to 178.7 MPa. It decreases the Crack Opening Development (COD) from 10.344 mm to 2.308 mm—the crack tip forms residual thermal stress, which protects crack initiation. Particle size, followed by reinforcement size, was the most vital factor in wear. However, it was noted that the sliding distance and load had an insignificant effect (John Iruthaya Raj et al., 2019).

The load has the utmost influence on the SWR value, whereas the reinforcement's impact is less. The Taguchi approach is efficient for predicting the SWR using wear experiments. (Stojanovic et al., 2017). DoE is centered on the L_{27} Taguchi OA. The impact of four regulating variables, namely, load, SiC content, D, and S, on the SWR of AMCs, is analyzed using an analysis of variance. The wear is found to be considerably affected by all the factors except sliding distance. The best combination of the four governing factors is also found for the least wear (Aliyu et al., 2020). The results of the wear tests show that the 98 percent Mg-2 percent SiC composite pin samples with higher hardness exhibit better wear resistance and friction force responses than other samples for all load and velocity parameters. SEM was used to evaluate the wear on the surface of the worn pin. (Kaviyarasan et al., 2019).

The wear properties of SiC-containing composites outperformed those of the matrix material (Selvaraj et al., 2021). Adhesive, abrasive, fretting, and wear delamination are all possible wear mechanisms in AMCs. Delamination is more common at peak loads in matrix alloys, whereas abrasion occurs at low loads in composites (Idusuyi and Olayinka, 2019). Composites beat unreinforced alloys up to 80 N loads with respect to wear resistance. The vol. percentage and particle size affect the wear of composites (Bhaskar et al., 2018; Meng et al., 2020). The key factors impacting the wear rate for all samples were load and reinforcement ratio, followed by sliding velocity.

On the other hand, the sliding distance does not affect the SWR (Chavhan and Wankhade, 2020). The Taguchi method points out the effect of variables on wear. Sliding speed and graphite content affect wear rates, followed by contact load (Miloradović et al., 2021). Under various parameters, the wear resistance is optimized. SEM images of worn-out surfaces were used to define the wear process of the composites. Taguchi technique is used to optimize the tribology parameters, resulting in the optimal set of input parameters (Vithal et al., 2021).

This manuscript describes the importance of combining hybrid AMCs with ceramic materials B4C and fly ash. It is a more suitable material for several applications where a high strength-to-weight ratio is required for the mechanical components. Pin-on-disc dry sliding wear tests were conducted using L_{27} OA for the wear behavior studies. The novelty of this research work is that the LM6/B4C/Fly Ash hybrid composites with three different weight percentages of reinforcement are fabricated using stir casting, and the experiments were conducted based on the DoE approach and optimized using Taguchi's S/N analysis.

The main objective this study is to fabricate LM6/B4C/Fly Ash hybrid composites using stir casting technique and to study the effect of wear process parameters by Taguchi's Design of Experiments using Pin-on-Disc wear testing apparatus and to analyze using S/N analysis. The microstructural analysis of the fabricated composites as well as the worn pin was done; also the hardness and density measurements of the hybrid composites were performed.

2 Literature survey

Al 7,178 aluminum alloy and nano titaniumdiboride is fabricated by Priyanka et al. (Priyanka et al., 2022). They used liquid state stir casting and examined the impact of wear parameters such as L, S, and D. They employed a powder addition with 2, 4, and 6 wt% to increase process control. Whenever the D is 2,250 m, and the sliding speed is 3 m/s, the wear rate is less. 20 kg of load, 1 m/s of sliding speed, 1,500 m of sliding distance, and a maximum COF. Because of their great wear resistance, engine parts, including piston rings, cylinders, and bearings, have demonstrated a particular interest in metal composites reinforced with titaniumdiboride particles.

With varying concentrations of zirconium oxide particles (0, 2, 4, and 6 wt%) while maintaining a constant 8 wt% Si_3N_4 particle content, the $Al7075/Si_3N_4/ZrO_2$ composites were created using the stir casting method by Anand Singh Rathaur et al. (Rathaur et al., 2019). The investigation's findings lead to the subsequent deductions. The tensile strength of the $Al7075/Si_3N_4$ composite was increased from 102.74 MPa to 130.71 MPa by the inclusion of ZrO_2 particles. With the addition of zirconia reinforcement, the

TABLE 1 Constitution of aluminum alloy (LM6).

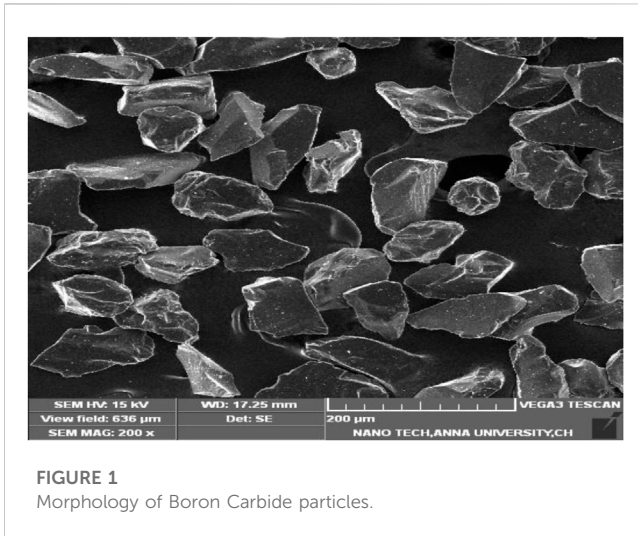| Constituent	Si	Cu	Fe	Mg	Mn	Ti	Ni	Zn	Al
Weight %	11.48	0.013	0.52	0.02	0.01	0.02	0.01	0.01	Remainder

FIGURE 1
Morphology of Boron Carbide particles.

ductility was further reduced. Furthermore, the inclusion of ZrO_2 particles enhanced the composites' hardness from 74.66 HRB to 81.4 HRB. The crystalline structure in an aluminum matrix reveals an arrangement of boundaries of grains everywhere as well as an inter-dendritic network of zirconia and silicon nitride particles. In comparison with an aluminum alloy without reinforcement, reinforcement provides a significant improvement in the wear characteristics. According to the findings that were obtained and compared, it is found that hardness decreases as zirconia content rises.

Al2219, Al2219+ Si_3N_4 + nano-Gr, and Al2219+ TiB_2 + nano-Gr composites were produced through stir casting using L_{27} OA by Chandrasekhar et al. (Chandra et al., 2022). The subsequent conclusions are feasible to reach. At any temperature, the rate of wear increases as the L and S increase. (ii) The AMC tribolayers' wear rate was greatly impacted. The Al2219 samples had the highest wear rates, whereas the titaniumdiboride and graphite-reinforced AMCs had the lowest. (iii)It is also recognized that sliding leads to adhesive and abrasive wear. The outcomes demonstrated that TiB_2 and graphite-containing composites might replace Al2219 metal matrix composites (iv)The hybrid composite outperforms other composites regarding wear resistance. Since the tribolayer is solid, graphite and titanium dioxide tribolayers degrade slowly.

The major matrix material is copper, which is supplemented by Mo and SiC_p particles that have average diameters of 44 μm and 45–75 μm, composites Ø20 mm × 55 mm in size were created by powder metallurgy by Emine sap et al. (Şap et al., 2021). Mo and SiC_p reinforcement ratios of 0 weight percent, 5 weight percent, 10 weight percent, and 15 weight percent were used to prepare test samples. Throughout the manufacturing process, three of the metallic particles were first combined for about 180 min, followed by exposure to a cold press for about 5 min, and finally sintered for 60 min at 1,050°C. The sintering process employed inert gas (argon). With more

additions, the percentage ratios of Mo and SiC_p rise while the amount of copper context steadily decreases. As a result, as the copper ratio decreases, the part's overall hardness is increased by the hard particles that are there. Here, hardness measurements were made using a testing device (model: BMS) under a 10 s load that was less than 10 kg. To verify the accuracy of the surface-level responses, these measurements were carried out five times. It might be said that the impact of reducing parameters is minimal. As the reinforcement ratio rose, it was seen that the wear progress on the flank face occurred often due to the abrasive wear mechanism. As a result of adhesive and abrasive wear mechanisms, it can also be argued that built-up edges and craters are the primary tool failure kinds on the cutting tool's rake face. In rare circumstances, the ratio of hard particles influenced by reinforcement ratio can be the cause of various chipping and tool breakage developments. There is a propensity to choose the surface roughness according to the best characteristics, this can be offset by flank wear and cutting temperature.

Aluminum matrix composites (AMCs) wear behavior was examined by Udaya et al. (UdayaPrakash et al., 2020). AMCs comprise 3, 6, and 9wt% of fly ash as the reinforcement material and LM6 aluminum alloy as the matrix material. The AMCs were created by the stir casting method. Wear tests were performed on pin-on-disc following ASTM G99-05 standard. The Taguchi method was used, and the L_{27} OA was chosen for the wear experiments. The main goal is to explore the impact of WL, SD, SS, and R% on SWR using the S/N ratio and ANOVA. SWR is statistically most significantly impacted by load (24.31%), then sliding distance (16.43%).

The impact of production and machining parameters on the milling of Cu/BeCrC composites was evaluated by Usame et al. (Ali Usca et al., 2022), to study the connection between energy usage and cutting speed, feed rate, and reinforcing ratio. As a manufacturing indication for machine tools, the use of energy is influenced by a number of variables, including: i) cutting parameters like cutting speed, feed rate, and depth of cut; ii) the material qualities of the work piece; and iii) process variables such tool wear, cutting forces, etc. The consumption of energy increases dramatically when operation time is prolonged, highlighting the significance of the feed rate. Nevertheless, using the machine's tool at larger feed rates and depths of cut results in high cutting forces, and eventually reduces the necessary cutting power. High deformation rates are generated as a result of cutting at high cutting speeds, which leads directly to quick tool wear. High cutting forces and power result from excessive tool wear, although it should be remembered that faster cutting rates result in lower cutting power. Additionally, due to its impacts on wear texture, tribological conditions, surface morphology, and roughness during repetitive operations, work piece material requirements play a crucial part in the cutting mechanism. Determining the ideal settings is crucial because of these reasons and the intricacy of cutting procedures.

AMCs (AA 5083-SiC-Fly Ash) were made using the stir casting by Santhosh et al. (Santhosh et al., 2022a). The conclusions were

TABLE 2 Constitution of fly ash.

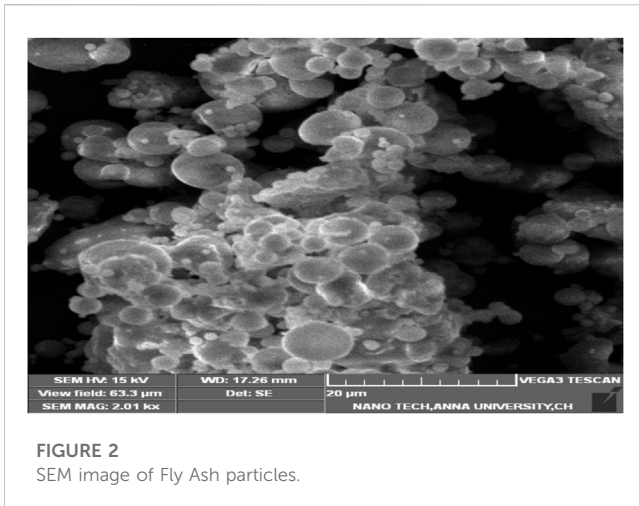| Constituent	Al	Si	O	Fe	Ti	K	Ca	LOI
Weight %	16.73	26.43	38.88	3.82	1.42	0.99	0.5	Remainder

FIGURE 2
SEM image of Fly Ash particles.

formed in light of the findings: Significant improvements in wear resistance are achieved by strengthening aluminum with SiC and FA and raising the amount of FA from 2.5% to 7.5%. The wear track notes a lesser wear rate with samples containing 7.5% fly ash. The influence of WL, SV, SD, and R% is determined by their proportion of influence for variation of WR and COF in the ANOVA. The experimental results and statistical predictions agree, and the error between them is within a band of 5%–10%. A careful examination of the relationship reveals that the wear rate lowers roughly 1.6 times as the Fly Ash percentage increases. This amply demonstrates how Fly Ash affected the wear samples.

To improve the various performance traits of LM25 hybrid composites, including WR and COF, Muthu employed (Muthu, 2020) Taguchi's OA with GRG. The following findings were reached through the current experimental work: The stir casting approach has effectively produced the AMCs. An even allocation of Cu and SiC is seen in the microstructural examination of the LM25 matrix alloy. Predicting the WR and COF of AMCs using the Taguchi approach is helpful. According to the results of the ANOVA, the SV (44.08%), SL (28.14%), and SD (27.53%) had the biggest effects wear properties of the AMCs. As the load increases, the wear rate rises. The inclusion of particles considerably increases the alloy's wear resistance. The composite unveils a lesser amount of wear over the matrix alloy itself.

Stojanovic (Stojanović et al., 2023) said the R%, S, and L have the greatest effects on wear, whereas the matrix material exhibits the greatest effects on friction. Uniform results unambiguously verify good particle dispersion and support using stir casting to create composite materials. The investigated materials' COF rose with the R%. The form of contact geometry and a significant decrease in the hardness of the tested material were the main causes of that rise. In the composite with 3 weight percent Gr, where the COF is maximum, there is a significant reduction in hardness.

Siddesh kumar (Siddeshkumar et al., 2015) revealed that with more R%, the SWR reduces; at room temperature, it is highest for Al2219 and minimal for Al2219 + 3%B_4C+5%MoS_2. The presence of reinforcements lowers the SWR of composite materials. The SWR of produced composites decreased by adding 3%, 4%, and 5% MoS_2 as secondary reinforcement. Examining the worn pin surfaces reveals wear mechanisms such as plastic deformation, delamination, and abrasion.

3 Materials and methods

3.1 Aluminium alloy (LM6)

Aluminum alloy (LM6) (Sargam Metals, Chennai) is used for wide applications like to withstand the high impact strength of hydraulic cylinders and less weight with the corrosion resistance of marine components, the thin, complicated component required to manufacture the precision alloy equipment is the critical area of this component. The chemical composition was found using optical emission spectroscopy is furnished in Table 1.

3.2 Boron carbide

The B_4C (Boron Carbide India Ltd., Mumbai) particles of 63 microns were used with desirable properties of high tensile strength, good hardness, and low density (Razzaq et al., 2021). It has high absorption of neutrons because the surface contains more cross-sections with low releasing radioactive isotopes. Experimented isotopes B^{10}cross section area is 755 barns. Figure 1 shows the morphology of the Boron Carbide (B_4C).

3.3 Fly ash

For this investigation, fly ash (Madras thermal power plant, Chennai) particles of 12 microns were used as added reinforcing material. Fly ash increases the hardness, wear resistance, damping qualities, and stiffness of aluminum alloys while lowering their density. Fly ash particles, accessible in huge amounts as an unneeded derivative of coal (thermal power plants) and are both low cost and low density, are prospective discontinuous dispersions used in metal matrix composite. The composition of FA is presented in Table 2. Figure 2 displays the morphology of FA.

3.4 Fabrication of LM6/B_4C/fly ash hybrid composites

LM6 ingots were heated in a furnace until they melted. Progressively, the temperature was increased to 850°C.

FIGURE 3
Stir casting Set up.

Hexachloroethane degasser was employed to degas the dissolved gases in the molten metal.

In order to add ceramic particles, the molten metal was swirled to form a vortex-like structure. The slurry is churned at 600 rpm for 7 min. In the hot metal, 1wt% K_2TiF_6 and Mg were applied. Ti and Mg were used to improve the wettability of B_4C-reinforced composites and fly ash-strengthened AMCs, respectively. 1.5, 3, and 4.5% of weight were added as B_4C%. Fly ash was incorporated at a weight proportion of 1.5, 3, and 4.5% for 3%, 6%, and 9% Hybrid Composites, respectively. After being poured into the mold, the slurry was allowed to cool to ambient temperature (Ananth et al., 2018; UdayaPrakas et al., 2018). Figure 3 depicts the stir casting apparatus used to create composites (Madras Institute of Technology, Anna University, Chennai).

3.5 Design of experiments

Using the Taguchi design of experiments approach, studies on the wear behavior of hybrid composites were conducted to test the significance of input variables on performance indicators and were analyzed using S/N analysis. Table 3 displays the process parameters and levels for conducting experiments.

Taguchi's quality philosophy is that quality should be designed into the product and not inspected into it. He suggested the use of Orthogonal Arrays (OAs) for designing the experiments. He has also developed the concept of linear graph which simplifies the design of OA experiments. These designs can be applied by engineers/scientists without acquiring advanced statistical knowledge. The main advantage of these designs lies in their simplicity, easy adaptability to more complex experiments involving number of factors with different number of levels. They provide the desired information with the least possible number of trails and yet yield reproducible results with adequate precision.

Steps in Taguchi methodology

Step-1: Identify the main function, side effects, and failure mode.

Step-2: Identify the noise factors, testing conditions, and quality characteristics.

Step-3: Identify the objective function to be optimized.

Step-4: Identify the control factors and their levels.

Step-5: Select the orthogonal array matrix experiment.

Step-6: Conduct the matrix experiment.

Step-7: Analyze the data; predict the optimum levels and performance.

Taguchi extended the audio concept of the signal to noise ratio to multi-factor experimental. The signal to noise ratio (S/N ratio) is a statistic that combines the mean and variance. The objective in robust design is to minimize the sensitivity of a quality characteristic to noise factors. This is achieved by selecting the factor levels corresponding to the maximum S/N ratio. That is, in setting parameter levels we always maximize the S/N ratio irrespective of the type of response (maximization and minimization). These S/N ratios are often called objective functions in robust design. The types of S/N ratios used in this research is smaller the better for COF and SWR.

Smaller the better: Here, the quality characteristic is continuous and non-negative. It can take any value between 0 to -∞. The desired value (the target) is zero. These problems are characterized by the absence of scaling factor (ex: surface roughness, specific wear rate, coefficient of friction, etc.). The S/N ratio (η) is given by

$$\eta = -10 \log\left[\frac{1}{n}\sum_{i=1}^{n} Y_i^2\right] \qquad (1)$$

where n is the number of replications and Y is the responses.

3.6 Pin on disc wear test

According to ASTM G 99–05, dry sliding wear testing occurred at ambient temperature (College of Engineering Guindy, Anna University, Chennai). The stir cast composites have been machined into pins (φ 6 mm and L 40 mm), and the SR is reduced to around 0.5 μm. AISI 4140 steel disc (φ 55 mm T 10 mm, 55 HRC) is employed as the counter face material. These discs have been machined and honed to have an SR of about 0.5 m. The prepared Specimen is shown in Figures 4, 5

TABLE 3 Input Parameters and their levels.

Level	Sliding speed, S (m/s)	Sliding distance, D (m)	Load, L (N)	Reinforcement, R (wt %)
1	1	500	15	3
2	1.5	1,000	30	6
3	2	1,500	45	9
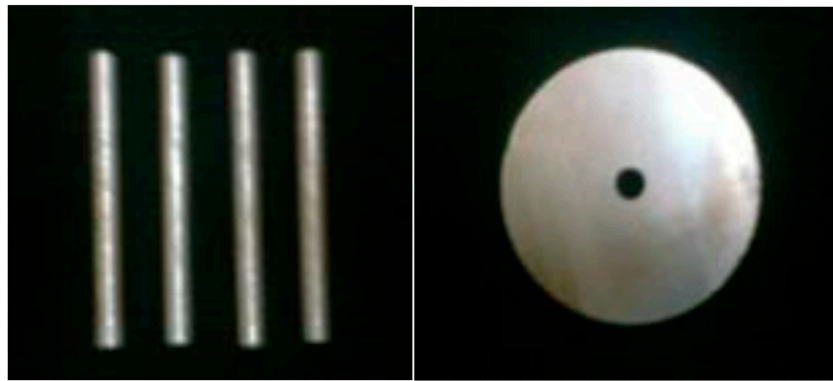
FIGURE 4
Photograph of prepared specimen (pins and disc).

FIGURE 5
Photograph of Pin on Disc equipment.

depicts the equipment used to study the composites' wear behavior.

The pin is firmly placed into its holder, the disc is attached to the rotating device, and the specimen is positioned perpendicular to the disk surface. The system lever is given more mass to create the desired force that presses the pin against the disc. The power source was turned on while holding the pin specimen away from the disc, and the speed was adjusted to the appropriate value. The appropriate time was entered into the timer. The samples are brought into contact beneath the load to begin the test. When the desired time has passed, the examination automatically ends. For determining volume loss, SWR, and COF, utilize Eqs 2–4.

$$Volume\,loss\,(V) = \frac{m_1 - m_2}{\rho} \, x \, 1000 \, mm^3 \qquad (2)$$

$$SWR = \frac{V}{L \, x \, D} mm^3 \Big/ Nm \qquad (3)$$

$$Coefficient\,of\,Friction\,(COF), \mu = \frac{F_T}{F_N} \qquad (4)$$

# 4 Result and discussions

4.1 Microstructural studies

Metallographic analysis is an investigative tool. An inverted optical microscope manufactured by Chennai Metco, India, was used for the microstructure analysis. Trials are taken from all four materials; their surface was made a mirror-like shine. The microstructural analysis aims to validate the reinforcement particles' uniform distribution. Micrographs are shown in Figure 6.

The optical microscopy technique studies the microstructure of the materials. The image is magnified 200 times, and the scale length shown in the micrograph is 50 μm. The spreading of particles in LM6 alloys is homogenous (Figure 6A). This characteristic homogenous distribution trend is maintained in LM6 alloys due to the greater silicon content. The eutectic constituents of LM6 are long acicular, script shape, and unchanged. Figure 6B shows the distribution of 3% (1.5% B4C and 1.5% fly ash) in the aluminum matrix hybrid composites. Figure 6C is the photomicrograph of a hybrid composite of LM6 alloys with 6% (3% B4C and 3% fly ash) hybrid composites. Figure 6D is the photomicrographs of hybrid composites of 9% (4.5% B4C and 4.5% fly ash). Boron carbide is black with an average particle size of 63 microns, and fly ash is grey with an average particle size of 12 microns; based on the dark and light colors and particle size, they are identified in the matrix.

4.2 Hardness test

Analog Rockwell hardness tester, manufactured by R.K. Instruments, Kohlapur, India, was used for testing the hardness. The hardness of AMCs and unreinforced alloys was assessed using the test scale E. The samples were ground to accurately determine the object's hardness, and measurements were made arbitrarily in 5 places for all materials (Zhao et al., 2020).

Figure 7 shows that the composites' hardness was higher than its base alloy's. Additionally, it has been discovered that when the reinforcement % increases, the composite's hardness rises (Ali et al., 2021). Adding hard particles increases the composites' resistance to plastic deformation and raises their hardness (Veeresh Kumar et al.,
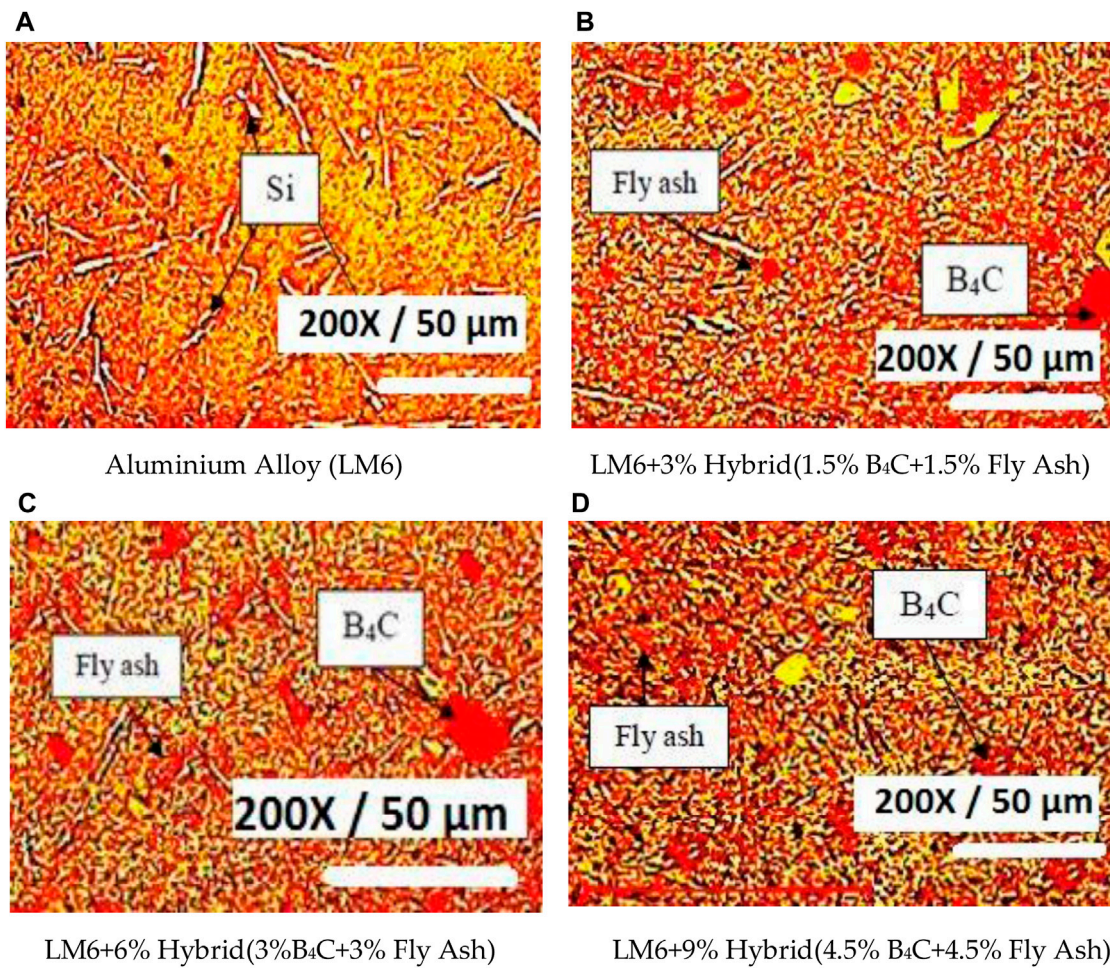
FIGURE 6
(A–D) Micrographs of B4C/Fly Ash reinforced hybrid AMCs.
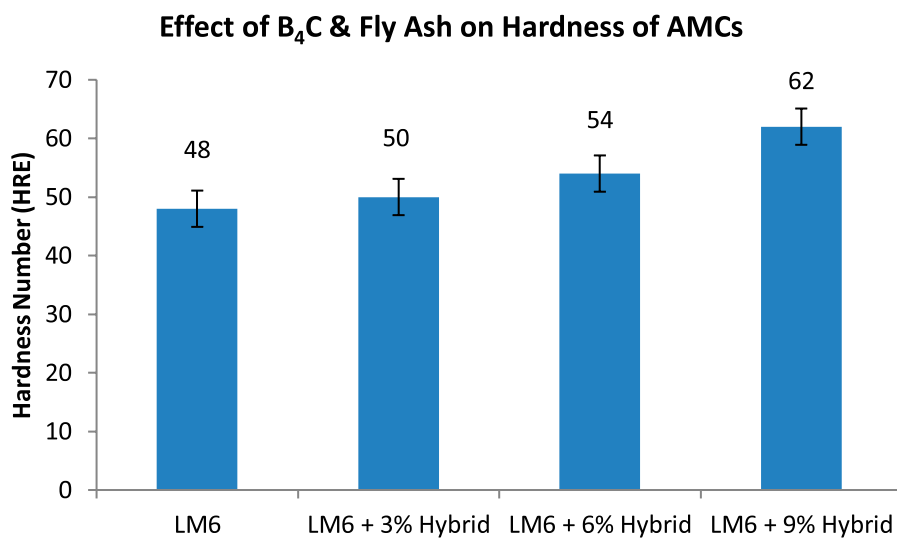
FIGURE 7
Effect of B4C& Fly ash on the hardness of AMCs.
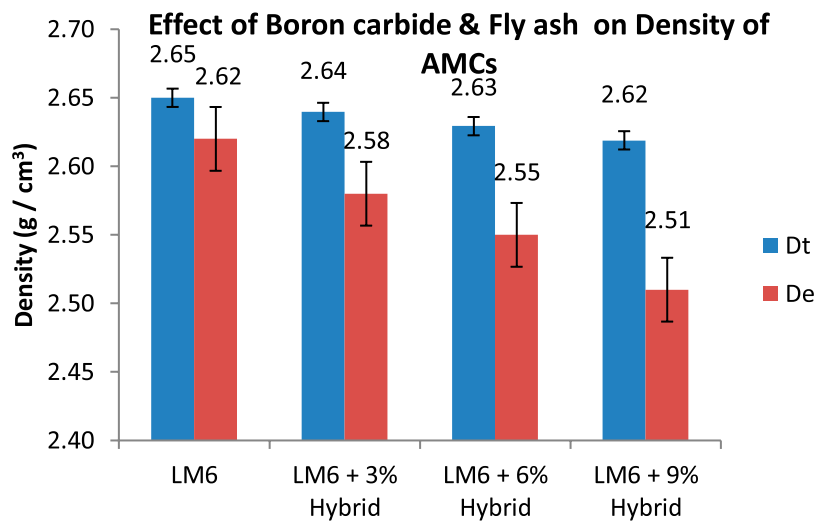
FIGURE 8
Effect of B$_4$C and Fly ash on the Density of AMCs.
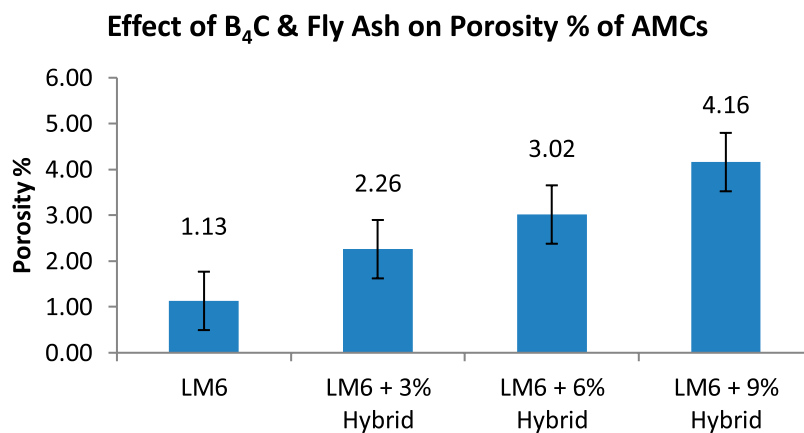
FIGURE 9
Effect of B$_4$C& Fly ash on the Porosity of AMCs.

2021). Adding fly ash particles, such as cenospheres and precipitators, causes a rise in hardness (HimaGireesh et al., 2018). Such tough reinforcing granules prevent plastic deformation. R % strengthens the matrix, raises the composite's degree of hardness, and prevents atom dislocation. An identical occurrence is noted by Mattli et al., 2021 (Mattli et al., 2021).

4.3 Density measurement

Density is the physical quality that most accurately reflects the characteristics of composites. The density of AMCs is empirically determined using Archimedes' principle. Electronic weighing equipment is used to measure the specimen's mass with a 0.001 g precision. By measuring the displacement of water with a cylinder with graduated levels, the total volume is determined. The materials density is determined using Equation (5).

$$Density = \frac{Mass}{Volume} \qquad (5)$$

Figure 8 shows that when the reinforcement % increases, the density of AMCs declines (Mohamed Ariff et al., 2022). The reason is that fly ash (2.09 g/cm^3) and B$_4$C (2.52 g/cm^3) have lower densities than an aluminum alloy (2.65 g/cm^3). Theoretical density calculated based on the rule of mixtures for 3% hybrid is 2.64 g/cm^3, 6% hybrid is 2.63 g/cm^3, and 9% hybrid is 2.62 g/cm^3. The experimental density also follows the same trend, but the porosity increases with the increase in reinforcement material due to the agglomeration of the ceramic particles. Regarding the material's overall dimension, porosity is the amount of voids in the substance. Vacuum dividing by the entire volume (vacuum/total) is an algebraic

TABLE 4 Experimental results of COF and SWR.

Expt. No.	Sliding speed, S (m/s)	Sliding distance, D(m)	Load, L (N)	Reinforcement, R (wt %)	COF	S/N for COF	SWR x 10^{-5} (mm^3/Nm)	S/N for SWR
1	1.0	500	15	3	0.408	7.79	9.78	80.19
2	1.0	500	30	6	0.404	7.87	5.12	85.81
3	1.0	500	45	9	0.334	9.53	10.15	79.87
4	1.0	1,000	15	6	0.525	5.60	10.25	79.79
5	1.0	1,000	30	9	0.211	13.51	5.08	85.89
6	1.0	1,000	45	3	0.299	10.49	3.26	89.73
7	1.0	1,500	15	9	0.342	9.32	10.15	79.87
8	1.0	1,500	30	3	0.579	4.75	9.78	80.19
9	1.0	1,500	45	6	0.453	6.88	10.25	79.79
10	1.5	500	15	6	0.198	14.07	10.25	79.79
11	1.5	500	30	9	0.207	13.68	5.08	85.89
12	1.5	500	45	3	0.292	10.69	9.78	80.19
13	1.5	1,000	15	9	0.404	7.87	25.38	71.91
14	1.5	1,000	30	3	0.287	10.84	7.34	82.69
15	1.5	1,000	45	6	0.417	7.60	10.25	79.79
16	1.5	1,500	15	3	0.386	8.27	11.41	78.85
17	1.5	1,500	30	6	0.326	9.74	9.39	80.54
18	1.5	1,500	45	9	0.414	7.66	9.02	80.89
19	2.0	500	15	9	0.328	9.68	10.15	79.87
20	2.0	500	30	3	0.406	7.83	12.23	78.25
21	2.0	500	45	6	0.4	7.96	5.12	85.81
22	2.0	1,000	15	3	0.485	6.29	12.23	78.25
23	2.0	1,000	30	6	0.312	10.12	7.68	82.29
24	2.0	1,000	45	9	0.399	7.98	5.92	84.55
25	2.0	1,500	15	6	0.283	10.96	13.66	77.29
26	2.0	1,500	30	9	0.512	5.81	11.00	79.18
27	2.0	1,500	45	3	0.456	6.82	9.78	80.19

proportion typically multiplied by 100 to allow comparisons in terms of percentages rather than decimals. Eq. 6 is utilized in the computation. The porosity of AMCs is shown in Figure 9.

$$\text{Porosity \%} = (\text{Theoretical Density} - \text{Experimental Density}) \times 100 \ /\text{Theoretical Density}$$

(6)

Similar density fluctuations are shown by earlier investigations and the findings (Mohammed Razzaq et al., 2020; Patnaik et al., 2022). Monolithic B$_4$C ceramic is an extremely stiff, robust, and hard low-density material. In order to create a strong low-density material, LM6-B$_4$C-Fly ash composites can conglomerate the very high stiffness and excellent hardness of B$_4$C with the Aluminium ductility (Choo et al., 2020; Ghandvar et al., 2021). From the density results, it can be interpreted that a reduction in density is required to fabricate lightweight composite materials.

4.4 Wear test results

The experimental findings on the wear characteristics of hybrid AMCs made of LM6/Boron Carbide/Fly Ash are presented in this section. COF and SWR are the main topics of examination and discussion. The optimal process parameters were selected based on Taguchi's S/N analysis, and confirmation tests were done. The wear test aims to determine how process parameters affect the COF and SWR. The L$_{27}$ OA was selected. The experimental results of COF, SWR, and S/N ratios of COF and SWR are tabulated in Table 4.
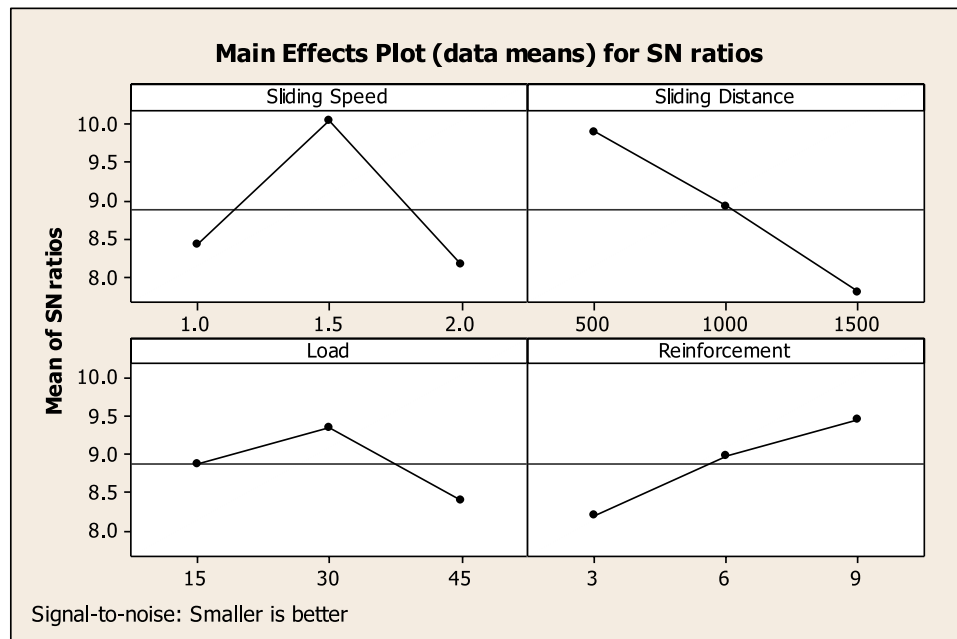
FIGURE 10
Response graphs for COF.

TABLE 5 Response table for COF.

Level	Sliding speed, S (m/s)	Sliding distance, D(m)	Load, L (N)	Reinforcement, R (wt %)
1	8.41	9.90	8.87	8.20
2	10.05	8.92	9.35	8.98
3	8.16	7.80	8.40	9.45
Delta	1.89	2.10	0.95	1.25
Rank	2	1	4	3

4.4.1 Analysis and discussion of results of COF

To verify the sliding parameter, L_{27} OA was employed, and its respective S/N graph was plotted in Figure 10. The COF decreases with a decrease in Sliding Speed, Sliding Distance, and load and decreases with the increase in R%. Higher sliding speed decreases friction since the transfer layer on the AMCs acts as an extra layer of protection and aids in COF reduction. The decrease in COF with the increasing load during sliding wear is caused by the accumulation of wear debris in the gaps between the pin and disc, resulting in a reduced effective penetration depth and finally switching the mechanism from 2-body to 3-body wear. The effect of D on COF is less substantial.

4.4.2 Selection of optimal levels

The optimal values are identified based on delta ranks shown in the S/N response in Table 5. According to the delta rank, the first dominating parameter is sliding Distance, followed by speed, reinforcement, and finally, load. The sliding speed shows a similar response in both SWR and the COF of the response graph. It can be seen from Figure 10 that the S_2, D_1, L_2, and R_3

provide optimum values. The F- table value at the 5% significance level is $F_{0.05, 2, 10} = 4.10$ and $F_{0.05, 4, 10} = 3.48$, so, from ANOVA Table 6, it is proved that the S, D, and DL were significant. Load and R % are combined into the error term.

4.4.3 Confirmation experiments for COF

The optimal parameter values are 1.5 m/s of S, 500 m of D, 30 N of Load, and 9% reinforcement. The COF confirmation test shows the slightest difference between the predicted value (0.248) and their respective experimented value (0.264).

4.4.4 Influence of process parameters on COF

Figure 11 shows the effect of process parameters on SWR. Low applied loads and sliding speeds result in lower friction coefficients because there is less transfer film generation at the interface. The production of transfer film happens quickly at greater sliding velocities. As a result, a slightly high friction coefficient is discovered. However, the production and degradation of the transfer film occur quickly at greater loads and speeds, resulting in a lower friction coefficient (Patnaik et al., 2022). The friction

TABLE 6 ANOVA for COF.

Source of variation	DOF	Sum of squares (SS)	Mean SS	F_o	Contribution (%)
S	2	18.84	9.42	4.11	12.50
D	2	19.85	9.93	4.33	13.17
DL	4	47.67	11.92	5.20	31.62
DR	4	16.66	4.17	1.82	11.05
LR	4	24.81	6.20	2.71	16.46
Error(Pooled)	10	22.92	2.29		15.20
Total	26	150.75			100

FIGURE 11
Effect of process parameters on COF.
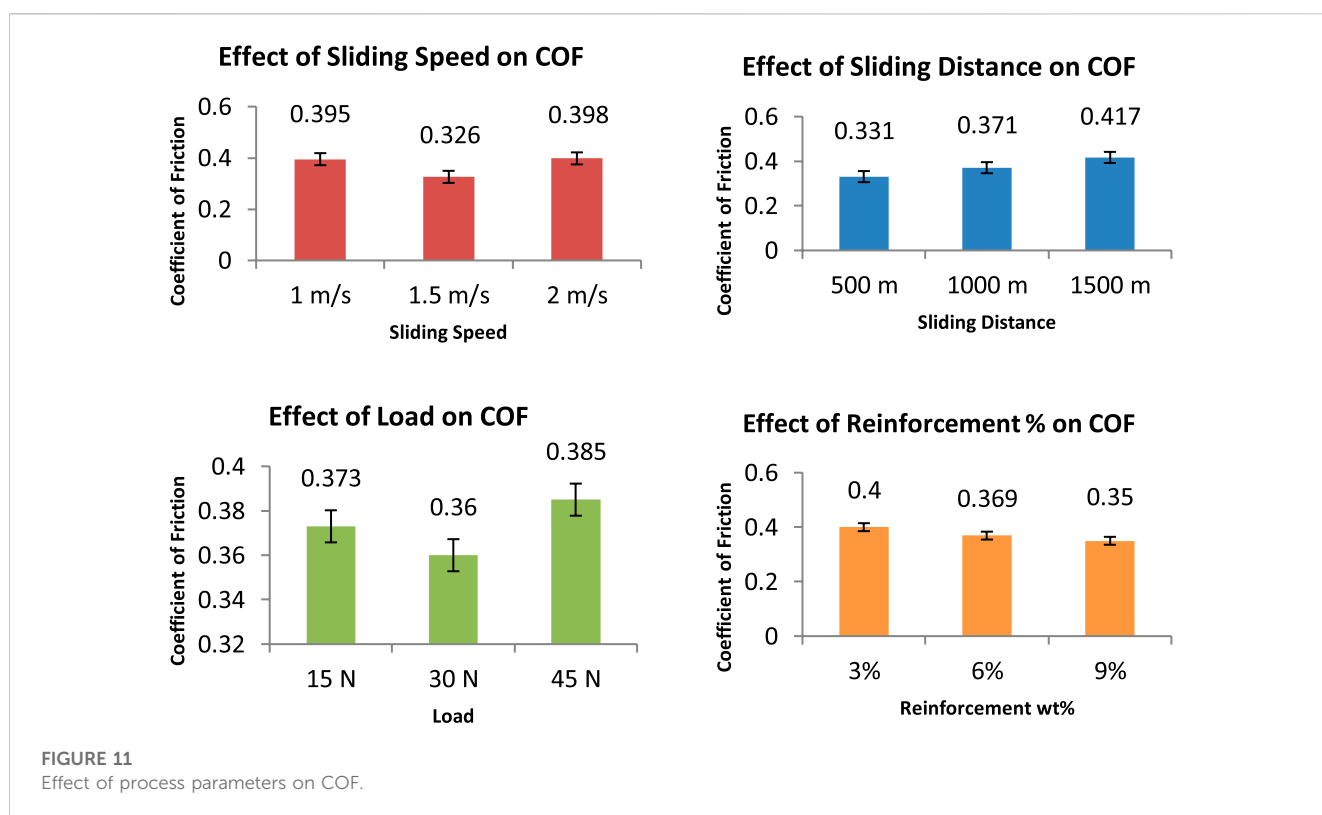
coefficient generally falls for high sliding speeds as the applied load rises. Notably, the load's impact on the SWR is just as strong as its impact on the COF (Uyyuru et al., 2007). A rise in L and S reduced the COF for a given R%. The same outcome was obtained by Ravi Kumar et al., who found that as the load rose, the COF dropped.

In conclusion, the COF dropped as the fly ash, load, and speed increased (Sviridenok et al., 2015). It has been found that increasing sliding velocity decreases the SWR and COF. It is hypothesized that the transfer layer on MMC serves as a protective layer, slowing down wear and reducing friction (Samal et al., 2020). The friction coefficient reduces with sliding speed increase (Bhuvaneswari et al., 2021). As the fly ash concentration has grown, the COF has decreased. With hard ceramics that provide abrasion resistance and an increased sliding distance, the coefficient of friction reduces, leading to

improved dry sliding wear performance (Rodiouchkina et al., 2018).

4.4.5 Analysis and discussion of results of SWR

The sliding wear trials were performed based on the Taguchi DoE technique with S, D, L, and R % as the process parameters and SWR and COF are the responses. The response characteristic of various levels was calculated, and their graph of S/N analysis was plotted based on the main effect of process variables. Prominent variables were identified using ANOVA of the S/N ratio, and the graphs were plotted based on the response table. The most prominent variable is easily visible from the graph, and their quantified optimal condition was recorded.

Figure 12 demonstrates that the SWR lowers with decreasing D, R%, and S and lowers with increasing load because the mechanically
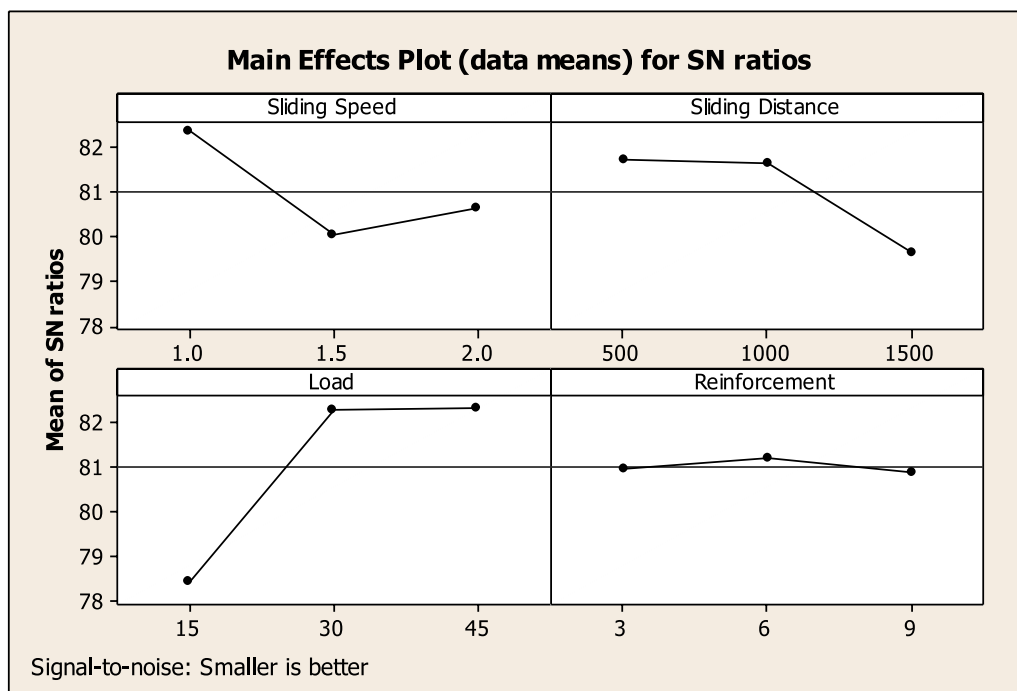
FIGURE 12
Response graphs for SWR.

mixed layer on the composite functions as a barrier to damage and aids in lowering SWR, higher sliding speeds result in reduced wear rates. The buildup of wear debris in the gaps between the pin and disc causes a reduction in the actual penetration depth, which finally converts the wear mechanism from 2-body to 3-body wear and causes the drop in SWR throughout sliding wear with the rise in load. On SWR, the impact of reinforcement is less significant. For the tested range, the sliding wear decreases as the sliding speed rises. This has been significantly linked to the Al alloy oxidizing due to higher interfacial temperatures. By reducing wear, the thicker oxide present protects the sliding interfaces. This could also cause the current situation's decreased SWR with increased S (Timelli et al., 2019). As the S increases, less time will be available for wear debris to escape from the worn track. This will indicate that the tribo-layer thickness grows with increasing sliding speed and will remain substantially thicker for extended periods. In conclusion, a stable tribo-layer protects the composites from excessive Wear Rate. This layer's formation is influenced by the extent of load, the S, the working temperature, and the MMC's composition. The reinforcement volume fraction is an essential factor. Materials with high hardness and sufficient fracture toughness are necessary to provide a decreased wear rate for the counter face (Santhosh et al., 2022b; Zaki et al., 2022).

4.4.6 Selection of optimal levels for SWR

Table 7 displays the mean of every response attribute (S/N data) for each level of every factor. According to delta statistics, which measure the relative amount of effect, the table comprises rankings. The difference between the largest and the smallest value is known as the delta statistic. Rankings are allocated according to delta values.

The one with the greatest delta value receives rank 1. The rankings show how important each aspect was about the outcome. According to the rankings and the delta values, the factors significantly affecting SWR are Load, S, D, and R%, in that order. Figure 12 demonstrates that the S_1, D_1, L_3, and R_2 offer the best results. ANOVA was conducted to investigate each process parameter's importance for lower SWR. The F-value from the table is $F_{0.05, 2, 8} = 4.46$ and $F_{0.05, 4, 8} = 3.84$ at the 5% significance level. As a result, we can see from ANOVA Table 8 that Load is the most important component. The error term contains reinforcement.

4.4.7 Confirmation experiment for SWR

The confirmation experiment and the SWR prediction are carried out using the ideal values. The analysis of experimental findings identifies the ideal values. The components at levels S_1, D_1, L_3, and R_2, S = 1 m/s, D = 500 m, L = 45 N, and R = 6%, are the ideal settings for minimal SWR, according to response Table 7; Figure 12. The experimental value of SWR is 5.14×10^{-5} mm³/Nm, while the predicted SWR is 5.28×10^{-5} mm³/Nm.

4.4.8 Effect of process parameters on SWR

The wear results are discussed based on the input parameters: L, S, D and R%. Figure 13 shows the effect of process parameters on SWR.

4.4.8.1 Effect of load on SWR

SWR of the AMCs rose when the load increased, and the abrasion and pressure increased (Alam et al., 2022; Balaji et al., 2022). The small broken ceramic fragments create a three-body abrasion that removes the material from the pin's surface. More

TABLE 7 Response table for SWR.

Level	Sliding speed, S (m/s)	Sliding distance, D(m)	Load, L (N)	Reinforcement, R (wt %)
1	82.35	81.74	78.42	80.95
2	80.06	81.65	82.30	81.21
3	80.63	79.64	82.31	80.88
Delta	2.29	2.10	3.89	0.33
Rank	2	3	1	4

TABLE 8 ANOVA for SWR.

Source of variation	DOF	Sum of Squares (SS)	Mean SS	F_0	Contribution (%)
S	2	25.51	12.755	2.76	7.99
D	2	25.35	12.675	2.75	7.94
L	2	90.53	45.265	9.81	28.34
SD	4	51.62	12.905	2.80	16.16
DL	4	45.5	11.375	2.47	14.24
DR	4	44.01	11.003	2.38	13.78
Error(Pooled)	8	36.91	4.614		11.55
Total	26	319.43			100

fragmented particles form as the load increases, and these particles flow through the pin (Soori and Asmael, 2022; Zaghloul et al., 2022). With an increase in the usual load, there has been more wear (Joseph et al., 2019; Subramaniam et al., 2019; Sathish and Karthick, 2020). Numerous researchers have reported on the influence of load on the SWR of MMCs. These experiments all showed that when the force applied increases, the rate of MMC wear also increases (Liu et al., 2019).

4.4.8.2 Effect of S on SWR

Consequently, as the speed rises, SWR and COF drop (Ghandvar et al., 2021). It has been found that increasing sliding velocity decreases the WR and friction coefficient. It is hypothesized that the transfer layer on MMC serves as a protective layer, slowing down wear and reducing friction (Choo et al., 2020). The SWR lowers as the S increases (Uyyuru et al., 2007; Patnaik et al., 2022). The conflicting effects cause the WR to decrease with raising S at low speeds. It is common knowledge that a material's hardness is influenced by how quickly it can be indented. The strain rate increases with an upsurge in sliding speed, enhancing the strength, and reducing the actual contact area, resulting in a lower wear rate. The heat rise brought on by friction causes the material to soften, another significant consequence of the increasing S (Sviridenok et al., 2015; Samal et al., 2020).

4.4.8.3 Effect of sliding distance on wear rate

Wear volume loss occurs as the sliding distance rises (Bhuvaneswari et al., 2021). This might be because the shattered particles trapped between the pin and the counter-face have a cutting capacity that does not diminish as the sliding distance

increases. While abrasive wear predominates in composites, adhesive wear is more common in unreinforced alloys (Rodiouchkina et al., 2018).

4.4.8.4 Effect of R% on SWR.

SWR was comparable at low sliding velocities, and the reinforcing did not affect the wear rate. The type of reinforcement used in steady-state sliding had no impact on the composite's wear rates (Patnaik et al., 2022). With a rise in reinforcing percentage, the wear rate declines. The counter face will be ploughed by the ceramic particles that the pin projects. The counter face's ploughed surface, which is made of Fe, will react with the pin's aluminum to generate Fe_2O_3, and ceramic particles will crush into microscopic particles to form a layer known as a mechanically mixed layer (MML). The MML creates a layer between the counter face and the hardened pin to lessen sliding wear. It will simply increase the MML's thickness; the amount of wear resistance improvement with additional reinforcement from 3 to 9 wt % in steps of 3% is smaller.

According to many researchers, the dry sliding wear resistance increases as the reinforcing content increases. The wear resistance increase will be reduced with additional increases in reinforcing content. The abrasion and fretting wear resistance of discontinuously reinforced aluminum (DRA) composites are improved by adding complex ceramic reinforcement up to around 20 vol%, according to Sannino and Rack (Timelli et al., 2019; Ghandvar et al., 2021).

Al-based MMC's wear and friction behavior are all exceedingly dependent on the reinforcement. The composites had high friction coefficients if a low MMC reinforcement particle rate. The volume
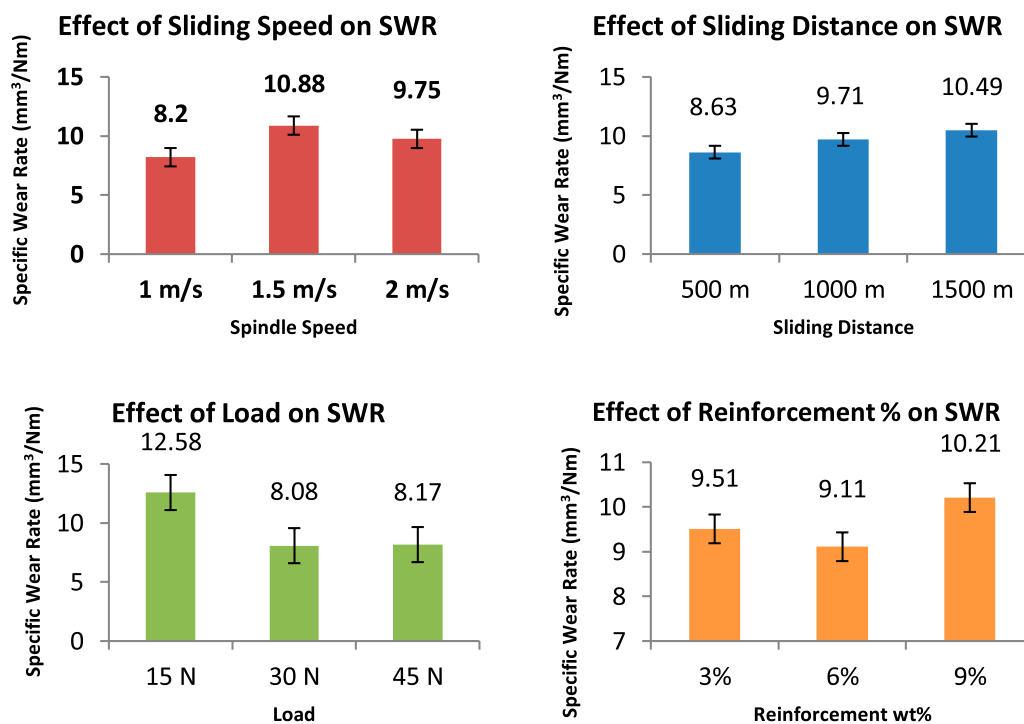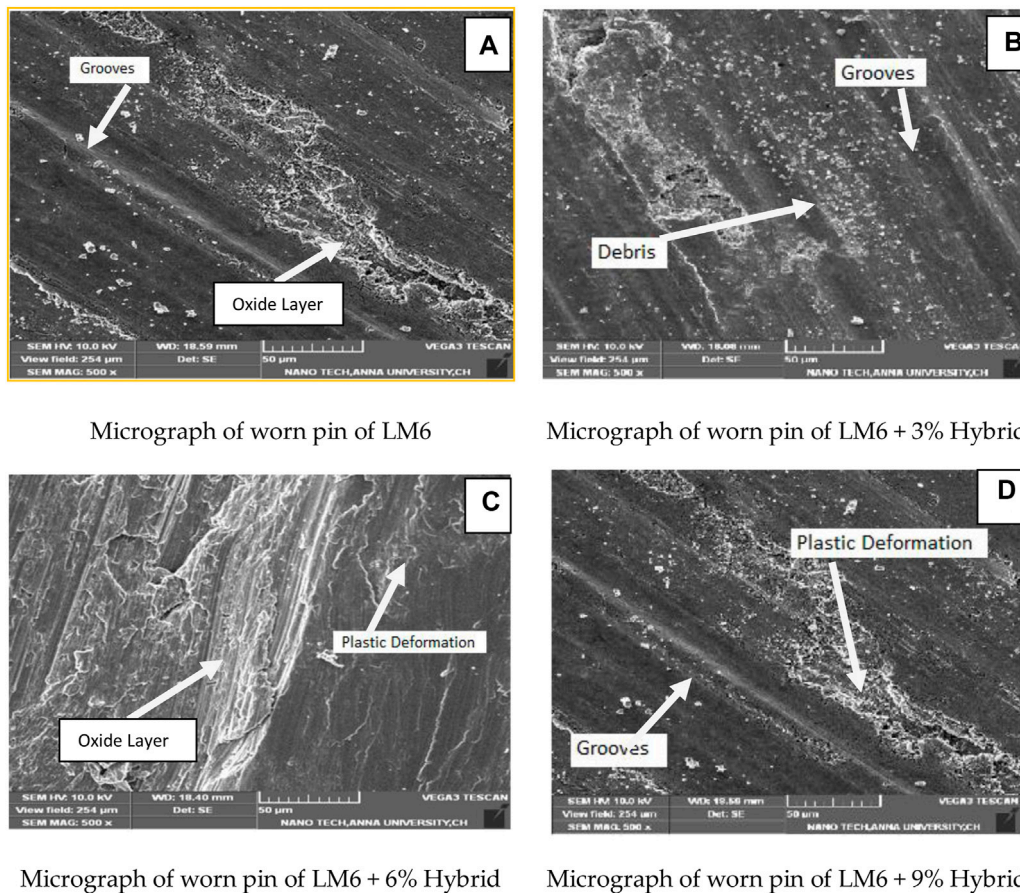
FIGURE 13
Effect of process parameters on SWR.

fraction of ceramics will continuously increase the wear resistance. This crucial volume fraction is influenced by the force used in the wear test (Zaki et al., 2022). Low wear rates were characterized by thin stable transfer layers and an almost constant wear coefficient; particle additions have decreased the SWR of the composites and delayed the transition with load from low wear coefficients to higher wear coefficients (Santhosh et al., 2022b). The MMCs with low fly ash weight percentages had significant wear, which grew linearly over time (Alam et al., 2022). At all speeds and loads, the wear volume reduced as the fly ash percentage increased (Balaji et al., 2022).

4.5 Micrographs of worn pins

Figure 14A show the SEM micrographs of worn pins of LM6 Al alloy. The presence of wear debris indicates the adhesive and plastic shearing of the asperities had occurred during the wear test (Radhika et al., 2015). Slighter grooves and wide-ranging patches in the sliding direction are visible in the SEM photos of the damaged surface of the LM6 Al alloy, signifying more significant wear and localized adhesion between the pin and the disc, likely caused by frictional heat forming the oxide layers. Figure 14B shows the SEM images of LM6+ 3% hybrid. The reinforcements act as abrasive against the counter face, increasing counter face wear. In addition, reinforcement liberated as wear debris acts as a third-body abrasive to both the composite and counter face surfaces (Rao et al., 2012). Due to their smaller dimensions and weaker nature than B_4C, fly ash particles are subject to plowing. Therefore, a comparison to virgin LM6 alloys reveals a lower wear rate. The

smaller friction and reduced wear rate may have been brought on by the presence of fly ash and boron carbide particles at the interface. Figure 14C shows the worn pin micrograph of LM6+6% Hybrid composite with decreased WR and ideal parameters. The worn surface shows plastic deformation and oxide layers. This reduction in the severity of the worn surfaces is due to the hard B_4C and fly ash particles which present direct contact of the matrix material with the more complex interface material. Figure 14D shows the worn pin micrograph of LM6 + 9% Hybrid composite with decreased WR. The micrograph shows small grooves and scratching on the composites' worn surface adjacent to the sliding path. In the SEM image, the fracturing of the oxide layers is readily apparent. The wear mechanism changes from abrasive wear to severe delamination wear as the load is increased. The change in wear mechanism from severe to mild wear can also be attributed to an increase in reinforcement content. Roy et al. (Roy et al., 2005) have observed that a reduction in the severity of plastic deformation due to the incorporation of hard reinforcement in an aluminium matrix. It is observed that an improvement in hardness was due to incorporation of hard reinforcements, resulting in increased wear resistance. As the speed increases, the contact time between the specimen and the counter face is very less and this results in lower material removal. As the wear proceeds, a work hardened layer consisting of iron from the counterface, aluminium and aluminium oxide from the specimen is formed on the surface of the pin and thus the wear mechanism changes from delamination wear to mild oxidative wear. Deuis et al. (Deuis et al., 1997) in the case of Al/SiC composites have observed that a MML was present on the worn surface of MMCs and this layer exhibited hardness approximately six times more than that of the bulk composite.

FIGURE 14
Micrograph of worn pins.

Micrograph of worn pin of LM6 (A)

Micrograph of worn pin of LM6 + 3% Hybrid (B)

Micrograph of worn pin of LM6 + 6% Hybrid (C)

Micrograph of worn pin of LM6 + 9% Hybrid (D)

5 Conclusion

With the help of the inexpensive stir casting procedure, hybrid composites were produced in three distinct weight percentages.

1) Optical micrographs confirmed that the reinforcement was distributed uniformly throughout the matrix.
2) Density and hardness were measured; LM6/9% hybrid has a low density and high hardness compared with other composites and base alloys.
3) Pin on disc, dry sliding wear tests were carried out on the hybrid composites using Taguchi's DoE and analyzed using S/N analysis.
4) The COF confirmation test shows the slightest difference between the predicted value (0.248) and their respective experimented value (0.264).
5) Load (28.34%) is the most significant variable, which has the ultimate statistical impact on SWR and Sliding distance on COF. SWR and COF decrease with a decrease in the sliding distance.
6) These experiments all showed that when the force applied increases, the rate of AMCs wear also increases.
7) While abrasive wear predominates in composites, adhesive wear is more common in unreinforced alloys.
8) Confirmation studies show a small margin of error for the responses. Between the expected and experimental values, there is a good agreement.
9) The hybrid composite produced is new and many new combinations may be produced and various optimization techniques may be used in future.
10) Initially the wear mechanism is two-body adhesive, and then it changes to abrasive wear due to the presence of ceramic reinforcements. The reinforcement increases the hardness of the composites and decreases the wear rate.

Data availability statement

The original contributions presented in the study are included in the article/Supplementary material, further inquiries can be directed to the corresponding author.

Author contributions

JU: Conceptualization, Investigation, Methodology, Software, Validation, Writing–original draft, Writing–review and editing, Resources. SA: Methodology, Software, Supervision, Writing–original

draft, Project administration, Resources. SJ: Formal Analysis, Methodology, Project administration, Validation, Visualization, Writing–original draft. RC: Validation, Writing–review and editing. NK: Investigation, Software, Supervision, Validation, Resources, Writing–review and editing. SS: Formal Analysis, Investigation, Methodology, Software, Writing–review and editing, Funding acquisition. EA: Funding acquisition, Resources, Validation, Visualization, Conceptualization, Formal Analysis, Software, Writing–original draft, Methodology. AK: Data curation, Methodology, Project administration, Supervision, Validation, Writing–original draft, Funding acquisition, Software.

Conflict of interest

The authors declare that the research was conducted in the absence of any commercial or financial relationships that could be construed as a potential conflict of interest.

Publisher's note

All claims expressed in this article are solely those of the authors and do not necessarily represent those of their affiliated organizations, or those of the publisher, the editors and the reviewers. Any product that may be evaluated in this article, or claim that may be made by its manufacturer, is not guaranteed or endorsed by the publisher.

References

Aherwar, A., Patnaik, A., and Pruncu, C. I. (2020). Effect of B$_4$C and waste porcelain ceramic particulate reinforcements on mechanical and tribological characteristics of high strength AA7075 based hybrid composite. *J. Mater. Res. Technology9* 5, 9882–9894. doi:10.1016/j.jmrt.2020.07.003

Alam, K. I., Garodia, A., Bragaw, P., and Burris, D. L. (2022). Independently tuning surface and subsurface reinforcement to optimize PTFE wear. *Wear* 510, 204516. doi:10.1016/j.wear.2022.204516

Ali, K. S. A., Mohanavel, V., Vendan, S. A., Ravichandran, M., Yadav, A., Gucwa, M., et al. (2021). Mechanical and microstructural characterization of friction stir welded SiC and B4C reinforced aluminium alloy AA6061 metal matrix composites. *Materials* 14 (11), 3110. doi:10.3390/ma14113110

Ali Usca, Ü., Şap, S., Uzun, M., Kuntoğlu, M., Salur, E., Karabiber, A., et al. (2022). Estimation, optimization and analysis based investigation of the energy consumption in machinability of ceramic-based metal matrix composite materials. *J. Mater. Res. Technol.* 17 (2022), 2987–2998. doi:10.1016/j.jmrt.2022.02.055

Aliyu, I. K., Azam, M. U., Lawal, D. U., and Samad, M. A. (2020). Optimization of SiC concentration and process parameters for a wear-resistant UHMWPE nanocomposite. *Arabian J. Sci. Eng.* 45, 849–860. doi:10.1007/s13369-019-04164-3

Ananth, S., Sivaprakasam, P., UdayaPrash, J., MaheanderaPrabu, P., Perumal, V., and Kalusuraman, G. (2021). Tribological behavior and surface characterization of gray cast iron-EN31 steel under lubricated sliding conditions. *J. Nanomater.* 2021, 1–9. doi:10.1155/2021/7725959

Ananth, S., UdayaPrakash, J., Moorthy, T. V., and Hariharan, P. (2018). Optimization of wear parameters for grey cast iron under different conditions using grey relational analysis. *Mater. Today Proc.* 5 (2), 7346–7354. doi:10.1016/j.matpr.2017.11.404

Balaji, S., Maniarasan, P., Alagarsamy, S. V., Alswieleh, A. M., Mohanavel, V., Ravichandran, M., et al. (2022). Optimization and prediction of tribologicalbehaviour of Al-Fe-Si alloy-based nanograin-refined composites using Taguchi with response surface methodology. *J. Nanomater.*, 2022, 1, 12. doi:10.1155/2022/9733264

Bhaskar, K. V., Sundarrajan, S., Rao, B. S., and Ravindra, K. (2018). Effect of reinforcement and wear parameters on dry sliding wear of aluminum composites-a review. *Mater. today Proc.* 5 (2), 5891–5900. doi:10.1016/j.matpr.2017.12.188

Bhuvaneswari, V., Rajeshkumar, L., and Ross, K. N. S. (2021). Influence of bioceramic reinforcement on tribologicalbehaviour of aluminium alloy metal matrix composites: experimental study and analysis. *J. Mater. Res. Technol.* 15, 2802–2819. doi:10.1016/j.jmrt.2021.09.090

Chandra, S., Gurusamy, P., Suthan, R., Melvin, V., Poures, D., Althahban, S., et al. (2022). Optimization on wear rate of aa2219/nanographite/TiB2/Si3N4 hybrid composites using taguchi process. *J. Nanomater.* 2022, 9. Article ID 1814623. doi:10.1155/2022/1814623

Chavhan, G. R., and Wankhade, L. N. (2020). Optimization of test parameters that influence on dry sliding wear performance of steel embedded glass/epoxy hybrid composites by using the taguchi approach. *Tribol. Industry* 42 (4), 556–571. doi:10.24874/ti.863.03.20.09

Choo, T. F., MohdSalleh, M. A., Kok, K. Y., Matori, K. A., and Abdul Rashid, S. (2020). Effect of temperature on morphology, phase transformations and thermal expansions of coal fly ash cenospheres. *Crystals* 10 (6), 481. doi:10.3390/cryst10060481

Deuis, R. L., Subramanian, C., and Yellup, J. M. (1997). Dry sliding wear of aluminium composites- A review. *J. Compos. Sci. Technol.* 57, 415–435. doi:10.1016/s0266-3538(96)00167-4

Ghandvar, H., Jabbar, M. A., Koloor, S. S. R., Petrů, M., Bahador, A., Bakar, T. A. A., et al. (2021). Role B4C addition on microstructure, mechanical, and Wear characteristics of Al-20% Mg2Si hybrid metal matrix composite. *Appl. Sci.* 11 (7), 3047. doi:10.3390/app11073047

HimaGireesh, C., Durga Prasad, K. G., and Ramji, K. (2018). Experimental investigation on mechanical properties of an Al6061 hybrid metal matrix composite. *J. Compos. Sci.* 2 (3), 49. doi:10.3390/jcs2030049

Idrisi, A. H., and Mourad, A. H. I. (2019). Wear performance analysis of aluminum matrix composites and optimization of process parameters using statistical techniques. *Metallurgical Mater. Trans. A* 50, 5395–5409. doi:10.1007/s11661-019-05446-z

Idusuyi, N., and Olayinka, J. I. (2019). Dry sliding wear characteristics of aluminium metal matrix composites: a brief overview. *J. Mater. Res. Technol.* 8 (3), 3338–3346. doi:10.1016/j.jmrt.2019.04.017

John Iruthaya Raj, M., Manisekar, K., and Gupta, M. (2019). Central composite experimental design applied to the dry sliding wear behavior of Mg/Mica composites. *J. Tribol.* 141 (1), 011603. doi:10.1115/1.4041073

Joseph, J., Haghdadi, N., Shamlaye, K., Hodgson, P., Barnett, M., and Fabijanic, D. (2019). The sliding wear behaviour of CoCrFeMnNi and AlxCoCrFeNi high entropy alloys at elevated temperatures. *Wear* 428, 32–44. doi:10.1016/j.wear.2019.03.002

Kaviyarasan, K., Soundararajan, R., Seenuvasaperumal, P., Sathishkumar, A., and Pradheep kumar, J. (2019). Experimental investigation of dry sliding wear behaviour on ceramic reinforced magnesium composite by powder metallurgy technique. *Mater. Today Proc.* 18, 4082–4091. doi:10.1016/j.matpr.2019.07.352

Liu, H., Liu, J., Chen, P., and Yang, H. (2019). Microstructure and high temperature wear behaviour of *in-situ* TiC reinforced AlCoCrFeNi-based high-entropy alloy composite coatings fabricated by laser cladding. *Opt. Laser Technol.* 118, 140–150. doi:10.1016/j.optlastec.2019.05.006

Mattli, M. R., Matli, P. R., Khan, A., Abdelatty, R. H., Yusuf, M., Ashraf, A. A., et al. (2021). Study of microstructural and mechanical properties of Al/SiC/TiO2 hybrid nanocomposites developed by microwave sintering. *Crystals* 11 (9), 1078. doi:10.3390/cryst11091078

Meng, Y., Xu, J., Jin, Z., Prakash, B., and Hu, Y. (2020). A review of recent advances in tribology. *Friction* 8, 221–300. doi:10.1007/s40544-020-0367-2

Miloradović, N., Vujanac, R., Stojanović, B., and Pavlović, A. (2021). Dry sliding wear behaviour of ZA27/SiC/Gr hybrid composites with Taguchi optimization. *Compos. Struct.* 264, 113658. doi:10.1016/j.compstruct.2021.113658

Mohamed Ariff, A. H., Jun Lin, O., Jung, D. W., MohdTahir, S., and Sulaiman, M. H. (2022). Rice husk ash as pore former and reinforcement on the porosity, microstructure, and tensile strength of aluminum MMC fabricated via the powder metallurgy method. *Crystals* 12 (8), 1100. doi:10.3390/cryst12081100

Mohammed Razzaq, A., Majid, D. L., Ishak, M. R., and MuwafaqBasheer, U. (2020). Mathematical modeling and analysis of tribological properties of AA6063 aluminum alloy reinforced with fly ash by using response surface methodology. *Crystals* 10 (5), 403. doi:10.3390/cryst10050403

Muthu, P. (2020). Multi objective optimization of wear behaviour of Aluminum MMCs using Grey-Taguchi method. *Manuf. Rev.* 7, 16. doi:10.1051/mfreview/2020013

Patnaik, L., Kumar, S., Gajjar, J., Dash, P., Maity, S. R., Łępicka, M., et al. (2022). Box–Behnken based investigation of surface quality and tool wear rate and FEM analysis of tool wear in TiAlN/CrN coated carbide tool. *Int. J. Interact. Des. Manuf. (IJIDeM)*, 1–16. doi:10.1007/s12008-022-01146-y

Priyanka, C., Parimala, P., Vishwanath Koti, N., Suganya Natarajan, M., Lakshmi narayana, K., and Arul, M. (2022). Optimization on TribologicalBehaviour of aa7178/nano titanium diboride hybrid composites employing taguchi techniques. *J. Nanomater.* 2022, 8. Article ID 1619923. doi:10.1155/2022/1619923

Radhika, N., Balaji, T. V., and Palaniappan, S. (2015). Studies on mechanical properties and tribological behaviour of LM25/SiC/Al2O3 composites. *J. Eng. Sci. Technol.* 10, 134–144.

Rao, C. S. P., Selvaraj, N., and Veeresh Kumar, G. B. (2012). Studies on mechanical and dry sliding wear of Al6061–SiC composites. *Compos. Part B* 43 (3), 1185–1191. doi:10.1016/j.compositesb.2011.08.046

Rathaur, A. S., Katiyar, J. K., and Patel, V. K. (2019). Experimental analysis of mechanical and structural properties of hybrid aluminium (7075) matrix composite using stir casting method. *IOP Conf. Ser. Mater. Sci. Eng.* 653 (1), 012033. doi:10.1088/1757-899x/653/1/012033

Razzaq, A. M., Majid, D. L., Basheer, U. M., and andAljibori, H. S. S. (2021). Research summary on the processing, mechanical and tribological properties of aluminium matrix composites as effected by fly ash reinforcement. *Crystals* 11 (10), 1212. doi:10.3390/cryst11101212

Rodiouchkina, M., Berglund, K., Mouzon, J., Forsberg, F., Ullah Shah, F., Rodushkin, I., et al. (2018). Material characterization and influence of sliding speed and pressure on friction and wear behavior of self-lubricating bearing materials for hydropower applications. *Lubricants* 6 (2), 39. doi:10.3390/lubricants6020039

Roy, D., Basu, B., and Mallick, A. B. (2005). Tribological properties of Ti-aluminide reinforced Al-based *in situ* metal matrix composite. *Intermetallics* 13, 733–740. doi:10.1016/j.intermet.2004.11.005

Samal, P., Vundavilli, P. R., Meher, A., and Mahapatra, M. M. (2020). Recent progress in aluminum metal matrix composites: a review on processing, mechanical and wear properties. *J. Manuf. Process.* 59, 131–152. doi:10.1016/j.jmapro.2020.09.010

Santhosh, M. S., Natrayan, L., Kaliappan, S., Patil, P. P., Rao, Y. S., Kumar, T. N., et al. 2022b. Mechanical and wear behaviour of nano-fly ash particle-reinforced mg metal matrix composites fabricated by stir casting technique. *J. Nanomater.*, 2022, 1, 8. doi:10.1155/2022/5465771

Santhosh, N., Praveena, B. A., Chandrashekar, A., Mohanavel, V., Raghavendra, S., and Basheer, D. (2022a). Wear behaviour of aluminium alloy 5083/SiC/fly ash inoculants based functional composites–optimization studies. *Mater. Res. Express* 9 (7), 076513. doi:10.1088/2053-1591/ac8229

Şap, E., Ali Usca, Ü., Gupta, M. K., Kuntoğlu, M., Sarıkaya, M., Yurievich Pimenov, D., et al. (2021). Parametric optimization for improving the machining process of cu/mo-sicp composites produced by powder metallurgy. *Materials* 14 (8), 1921. doi:10.3390/ma14081921

Sathish, T., and Karthick, S. (2020). Wear behaviour analysis on aluminium alloy 7050 with reinforced SiC through taguchi approach. *J. Mater. Res. Technol.* 9 (3), 3481–3487. doi:10.1016/j.jmrt.2020.01.085

Selvaraj, S. K., Raj, A., Dharnidharka, M., Chadha, U., Sachdeva, I., Kapruan, C., et al. (2021). A cutting-edge survey of tribological behavior evaluation using artificial and computational intelligence models. *Adv. Mater. Sci. Eng.* 2021, 1–17. doi:10.1155/2021/9529199

Siddeshkumar, N. G., Shiva Shankar, G. S., and Basavarajappa, S. (2015). A study on dry sliding wear behaviour of hybrid metal matrix composites at room temperature. *Appl. Mech. Mater.* 766, 219–228. doi:10.4028/www.scientific.net/amm.766-767.219

Soori, M., and Asmael, M. (2022). A review of the recent development in machining parameter optimization. *Jordan J. Mech. Industrial Eng.* 16 (2), 205–223.

Stojanovic, B., Blagojevic, J., Babic, M., Velickovic, S., and Miladinovic, S. (2017). Optimization of hybrid aluminum composites wear using Taguchi method and artificial neural network. *Industrial Lubr. Tribol.* 69, 1005–1015. doi:10.1108/ILT-02-2017-0043

Stojanović, B., Gajević, S., Miloradović, N., Nikolić, R., Miladinović, S., Svoboda, P., et al. (2023). Comparative analysis of hybrid composites based on A356 and ZA-27 alloys regarding their TribologicalBehaviour. *COMMUNICATIONS* 25 (3), B215–B227. doi:10.26552/com.c.2023.056

Subramaniam, B., Natarajan, B., Kaliyaperumal, B., and Chelladurai, S. J. S. (2019). Wear behaviour of aluminium 7075—boron carbide-coconut shell fly ash reinforced hybrid metal matrix composites. *Mater. Res. express* 6 (10), 1065d3. doi:10.1088/2053-1591/ab4052

Suresh, V. I. K. R. A. M., Vikram, P., Palanivel, R., and Laubscher, R. F. (2018). Mechanical and wear behavior of LM25 Aluminium matrix hybrid composite reinforced with Boron carbide, Graphite and Iron oxide. *Mater. Today Proc.* 5 (14), 27852–27860. doi:10.1016/j.matpr.2018.10.023

Sviridenok, A. I., Myshkin, N. K., and Kovaleva, I. N. (2015). Latest developments in tribology in the journal Friction and Wear. *J. Frict. Wear* 36, 449–453. doi:10.3103/s106836661506015x

Timelli, G., Fabrizi, A., Vezzù, S., and De Mori, A. (2019). Design of wear-resistant diecast AlSi9Cu3 (Fe) alloys for high-temperature components. *Metals* 10 (1), 55. doi:10.3390/met10010055

UdayaPrakash, J., Ananth, S., Sivakumar&T, G., and Moorthy, V. (2018). Multi-objective optimization of wear parameters for aluminium matrix composites (413/B4C) using grey relational analysis. *Today Proc.* 5 (2), 7207–7216. doi:10.1016/j.matpr.2017.11.387

UdayaPrakash, J., DivyaSadhana, A., Ananth, S., and ArunPillai, K. V. (2020). Optimization of wear parameters of aluminium matrix composites (LM6/Fly Ash) using Taguchi technique. *Mater. Today Proc.* doi:10.1016/j.matpr.2020.05.550

Uyyuru, R. K., Surappa, MK., and Brusethaug, S. (2007). Tribological behavior of Al–Si–SiCp composites/automobile brake pad system under dry sliding conditions. *TribologyInternational* 40 (2), 365–373. doi:10.1016/j.triboint.2005.10.012

Veeresh Kumar, G. B., Pramod, R., HariKiran Reddy, R., Ramu, P., Kunaal Kumar, B., Madhukar, P., et al. (2021). Investigation of the tribological characteristics of aluminum 6061-reinforced titanium carbide metal matrix composites. *Nanomaterials* 11 (11), 3039. doi:10.3390/nano11113039

Venkatachalam, G., and Kumaravel, A. (2017). Mechanical behaviour of aluminium alloy reinforced with SiC/fly ash/basalt composite for brake rotor. *Polym. Polym. Composites25* 3, 203–208. doi:10.1177/096739111702500304

Vithal, N. D., Krishna, B. B., and Krishna, M. G. (2021). Impact of dry sliding wear parameters on the wear rate of A7075 based composites reinforced with ZrB2 particulates. *J. Mater. Res. Technol.* 14, 174–185. doi:10.1016/j.jmrt.2021.06.005

Zaghloul, M. M. Y., Steel, K., Veidt, M., and Heitzmann, M. T. (2022). Wear behaviour of polymeric materials reinforced with man-made fibres: a comprehensive review about fibre volume fraction influence on wear performance. *J. Reinf. Plastics Compos.* 41 (5-6), 215–241. doi:10.1177/07316844211051733

Zaki, E. G., Selim, M. S., Hao, Z., ElSaeed, S. M., and El-Saeed, A. M. (2022). Special issue: recent trends in wear and erosion resistance of alloys. *Coatings* 13 (1), 64. doi:10.3390/coatings13010064

Zhao, Y., Yu, T., Sun, J., and Jiang, S. (2020). Microstructure and properties of laser cladded B4C/TiC/Ni-based composite coating. *Int. J. Refract. Metals Hard Mater.* 86, 105112. doi:10.1016/j.ijrmhm.2019.105112

Nomenclature

AISI	American Iron and Steel Institute
Al	Aluminium
AMCs	Aluminium Matrix Composites
ANOVA	Analysis of Variance
B4C	Boron Carbide
COF	Coefficient of Friction
DoE	Design of Experiments
FESEM	Field Emission Scanning Electron Microscope
LM	Light Metal
OA	Orthogonal Array
S/N	Signal to Noise Ratio
SEM	Scanning Electron Microscope
SiC	Silicon Carbide
SWR	Specific Wear Rate
XRD	X Ray Diffraction